High energy laser-wakefield collider with synchronous acceleration

C. Chiu,[1] S. Cheshkov,[1] and T. Tajima[1,2]

[1]*Department of Physics, University of Texas at Austin, Austin, Texas 78712*
[2]*Lawrence Livermore National Laboratory, Livermore, California 94550*

A recent study on a high energy accelerator system which involves multistage laser wakefield acceleration shows that the system is very sensitive to jitters due to misalignment between the beam and the wakefield. In particular, the effect of jitters in the presence of a strong focusing wakefield and initial phase space spread of the beam leads to severe emittance degradation of the beam. One way to improve the emittance control is to mitigate the wakefield by working with a plasma channel. However, there are limitations in this approach. Our present investigation does not involve a plasma channel. Instead of averaging over the full phase range of the quarter-wave acceleration, we treat the phase range as a variable. We have found that, for a fixed final acceleration energy and a small phase slip, the final emittance is inversely proportional to the total number of stages. This leads us to consider an accelerator system which consists of superunits, where each superunit consists of closely spaced short tubes, or chips, with the wakefield of each chip being created by an independent laser pulse. There is a relatively large gap between adjacent superunits. With this arrangement the beam electrons are accelerated with a small phase slip; i.e., the phase of the beam is approximately synchronous with respect to the wakefield. This system is designed to have resilience against jitters. It has its practical limitations. We also consider a "horn model" with an exact synchronous acceleration based on a scheme suggested by Katsouleas. Computer simulation of both the chip model and the horn model confirms an expected $(\sin\psi)^{3/2}$ law for emittance degradation in the small phase angle region. Thus the choice of a small loading phase together with a small phase slip provides another important ingredient in controlling emittance degradation.

I. INTRODUCTION

The concept of laser wakefield acceleration was originally proposed by Tajima and Dawson [1]. Since then there has been much research in this area. For a recent review, see Esarey *et al.* [2]. It is well known that the phase of laser-wakefield waves which is suitable for particle beam acceleration occurs within one-quarter of a wavelength, where there is a positive longitudinal force and, at the same time, the focusing force in the transverse direction. During the course of acceleration, the beam particles are slipping forward and eventually move out of the quarter-wave region. This ends a given acceleration stage.

In pursuit of the next energy front, a laser-based wakefield linear collider at high energies (such as 5 TeV) has been considered for which many wakefield units are needed to reach the desired energy. Also, the collider demands an extremely small emittance and thus extremely precise beam handling. In order to evaluate the potential of this approach to identify the crucial physical and technological problems associated with this, a systems approach through a dynamical map has been introduced [3–5]. There was also an earlier study on a 5 TeV laser-wakefield collider [6]. Emittance degradation in TeV accelerators for the case of a full fragmentation in the transverse phase space was considered in Ref. [7].

In Ref. [5], the study of emittance degradation in the presence of jitters, which may be associated with stochastic misalignment between the beam and the wakefields, was carried out where the plasma medium is uniform and the beam is accelerated over a full quarter-wave region. One finds that the system is relatively sensitive to jitters. This is due to the fact that the wakefield averaging over the entire accelerating phase has a strong focusing property.

A possible way to decrease the strong focusing wakefield is to work with a hollow channel design [8]. A drawback is that, due to the finite density gradient near the wall of the cavity, there is local plasma frequency which would match the wakefield frequency. This could lead to resonance absorption [9]. In Ref. [5], numerical models where beam acceleration was over a full quarter-wave region were considered. These models are for both without involving the plasma channel and with the plasma channel ignoring the resonance absorption effect. The former will be referred to as the CTHY model and the latter the CTHY1 model.

From a general consideration, one expects that the emittance degradation should depend on the phase range through which the acceleration occurs. In this work we will confine our attention to only the nonchannel case. In this context the present work is a sequel of the CTHY model. Using two different approaches we will explore ways to improve the resilience against jitters through variations over the loading phase and also over the phase interval of acceleration.

Our starting point is to fix the loading phase at some specific value and vary the spatial interval of acceleration. Since the total acceleration energy interval is fixed, a variation of the acceleration interval leads to the corresponding variation in the number of total acceleration units. Computer simulation indicates that, when the acceleration phase is approximately fixed, this occurs when the phase slip is small, so there is an inverse power behavior. In particular, the emittance degradation decreases as $1/N$, where N is the total number of acceleration units [10]. This confirms the theoretical expectation of CTHY deduced from a statistical theory [5]. The inverse power law suggested that through the use of small acceleration intervals one may be able to achieve high resilience against jitters. The spatial interval considered presently is of the order of 1 cm. It can be even much smaller. We conjecture that the active [11,12] photonic-crystal or photon-cell technology [13,14] may someday be used as basic units in a high energy laser-wakefield accelerator.

The second approach is to work with a synchronous acceleration model, where there is no phase slip at all. It was pointed out by Katsouleas [15] over a decade ago that synchronous acceleration can be achieved by varying the plasma density. More specifically, consider the case where the local density along the beam direction is gradually increasing. Then the wavelength of the plasma waves, on which the beam electrons are riding, becomes shorter and shorter. If the rate of the phase slip of the beam electrons exactly matches the rate of the phase advance due to the shrinkage of the plasma waves, a continuous acceleration without any phase slip may be achieved.

From a study on the hydrodynamics of nozzle flow [16], we find that, if there is a steady flow opposite to the direction of the beam, by fine tuning the increase of the nozzle cross section along the beam one can control the corresponding increase of the plasma density and in turn achieve a synchronous acceleration. Here the acceleration unit has a horn shape. We refer to this model as the "horn model," although in practice the increase of the radius of the cross section in some instances may be small.

Based on the Katsouleas matching condition, we have derived a set of analytic expressions which have been incorporated in the dynamical map. Our work here also takes into account the conservation of energy in the context of the pump-depletion effect [17] and the adiabatic invariance property throughout the acceleration process [18]. Our computer simulation for the horn model with a small loading phase shows a definite improvement over CTHY model.

The outline of the remainder of the present paper is as follows. In Sec. II, we review the basic formalism in laser-wakefield acceleration which establishes the convention and the notations used in the present work. Magnets will also be included in the system. In Sec. III, we present numerical results for a simple multistage model which confirms the approximate $1/N$ behavior. In the same section,

we review the stochastic theory on the emittance degradation, which serves as the basic framework in our emittance degradation analysis. In Sec. IV, we present basic setup and the numerical results on the approximately synchronous model, i.e., a system with superunits and chips. In Sec. V, we consider a synchronous model, where horns are basic units. Here, both the analytic expressions for the model and our numerical results will be presented. We conclude with a summary and discussion in Sec. VI.

II. MOTION OF BEAM PARTICLES

In this section we will review the basic formalism of laser-plasma acceleration [19] and the dynamical map introduced by CTHY [5]. For brevity we will simply state the essential points and leave out the nuances of the assumptions and justifications to these references. The CTHY map provides a convenient frame for the inclusion of magnets. In later sections, we will incorporate superunits with chips and also incorporate the exact synchronous system with horns into the map.

A. Laser pulse and wakefield

Laser pulse. Consider a laser pulse with a group velocity v_g traversing through a uniform plasma medium along, say, the z direction. In terms of the longitudinal coordinate variable defined in the frame comoving with the laser pulse $\zeta = z - v_g t$, the normalized vector potential is assumed to take on the form,

$$a(r, \zeta) = \frac{eA}{mc^2} = \begin{cases} a_0 f(\zeta)g(r), & \text{for } 0 \le \zeta \le L, \\ 0, & \text{otherwise.} \end{cases} \quad (1)$$

Here m is the electronic mass and L is the pulse length. The pulse longitudinal profile function $f(\zeta)$ may take on the form of a Gaussian shape (see, e.g., Ref. [5]). For the present theoretical discussion we will work with the sine form; i.e.,

$$f(\zeta) = \sin\frac{\pi\zeta}{L}.$$

The transverse cutoff function is assumed to be

$$g(r) = \exp\left(-\frac{r^2}{r_s^2}\right),$$

with r the transverse radius, i.e., $r^2 = x^2 + y^2$, and r_s the laser spot size. We assume x and y to be independent variables. For definiteness we will work with the x component.

Ponderomotive potential. It can be shown that the laser pulse generates a trailing Ponderomotive potential

$$\phi = \phi_{\max}g^2(r)\sin k_p\zeta, \quad (2)$$

$$\phi_{\max} = \frac{\Phi_0 E_{bk}}{k_p}, \quad \Phi_0 = \frac{\pi a_0^2}{4}, \quad E_{bk} = k_p\frac{mc^2}{e}.$$

The traveling speed of the plasma waves is the same as the group velocity of the laser pulse; i.e., $v_p = v_g$. Here E_{bk} is referred to as the Tajima-Dawson wakefield [1]. Consider the oscillation of a plasma medium. Poisson's equation implies that the amplitude of the wakefield is proportional to the amplitude of the plasma density variation. E_{bk} is the field strength where this relation breaks down in the nonrelativistic case. This occurs at the point where the amplitude of density variation in the waves equals the quiescent density. The specific form of Φ_0 is sensitive to the pulse shape $f(\zeta)$ assumed.[1] Denote the phase of the plasma waves by $\psi_p = k_p \zeta$, the traveling wakefield in the longitudinal and the transverse directions are respectively given by

$$E_z = -\frac{\partial \phi}{\partial z} = -E_{z0} g^2(r) \cos\psi \quad \text{with } E_{z0} = \Phi_0 E_{bk}, \tag{3}$$

$$E_x = -\frac{\partial \phi}{\partial x} = E_{x0} g^2(r) \sin\psi \quad \text{with } E_{x0} = \frac{4x}{r_s^2} \frac{\Phi_0 E_{bk}}{k_p}. \tag{4}$$

We proceed to consider the acceleration of a beam electron by the wakefield.

B. Longitudinal iterative map

Longitudinal variables. The longitudinal motion of a beam electron is specified by two variables (a) the longitudinal Lorentz factor γ associated with a speed $v = \beta c$ and (b) the longitudinal phase given by

$$\psi = \psi_s + k_p(z - v_g t). \tag{5}$$

At $t = 0$, the center of the beam is loaded at $z = 0$ where the plasma wave has a phase $\psi_p = \psi_s$. In the frame comoving with the plasma waves, the location where the phase is ψ_s will remain fixed. The beam is moving with a speed $v = \beta c$, which is close to the speed of light. The corresponding particle phase is given by $\psi(z,t) = \psi_s + k_p(\beta ct - v_p t)$. Thus, as an electron is riding on the wakefield waves, at time t the corresponding phase slip is given by $k_p(\beta - \beta_p)ct$.

Longitudinal equations of motion. In the z direction, the Lorentz force $F_z = mc\frac{d\gamma}{dt} = -eE_z$. This Lorentz force and the corresponding x component force are shown in Fig. 1(a). Taking $\psi_s = 0$ and neglecting the longitudinal

---

[1]For the sine form assumed, the coefficient of a_0^2 is $\sqrt{\pi/4} = 0.89$. For a Gaussian shape, if there is no restriction on its spatial extent, the corresponding numerical value is $\sqrt{\pi/2e} = 0.76$.
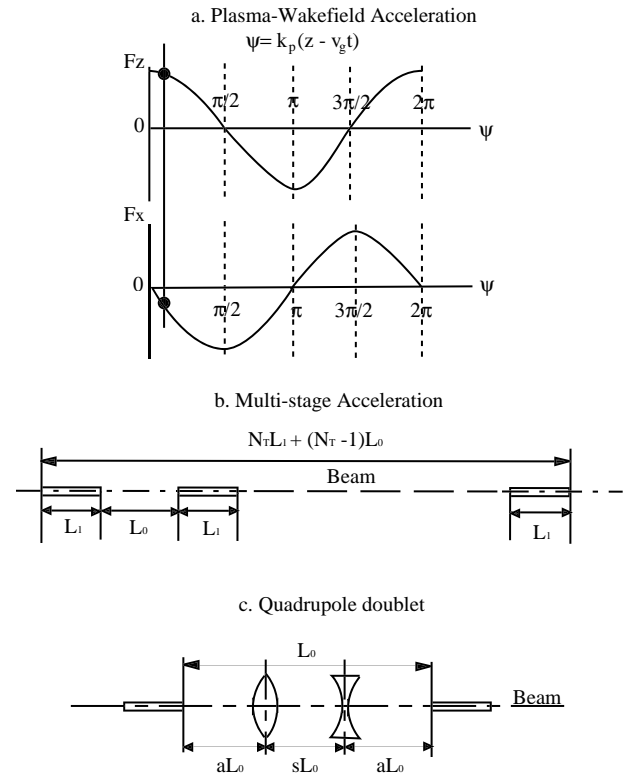
FIG. 1. Schematic illustrations of laser-wakefield acceleration. (a) Lorentz force F_z and F_x on a beam particle as a function of wakefield phase, (b) the layout of multistage acceleration, and (c) the layout of a quadrupole doublet in the gap.

spread of the beam, the appropriate quarter-wave region for beam acceleration is $0 \leq \psi \leq \pi/2$. Near the beam line, which is at $r = 0$,

$$\frac{d\gamma}{dz} = \frac{d\gamma}{cdt} = \Phi_0 k_p \cos\psi,$$

and

$$\frac{d\psi}{dz} = k_p\left(1 - \frac{\beta_p}{\beta}\right) \approx \frac{k_p}{2\gamma_p^2} \quad \text{with } \gamma_p = \frac{\omega}{\omega_p}. \tag{6}$$

In a plasma medium, the laser pulse satisfies the dispersion relation

$$\omega^2 = \omega_p^2 + (k_p c)^2,$$

and the traveling speed of the plasma waves induced by the laser pulse is identical to its group velocity. One may identify γ_p to be the Lorentz factor for a dressed photon with a rest mass energy $h\omega_p/2\pi$ (h being the Planck constant) and with a speed v_p, the plasma wave speed.

Iterative map. Consider the multistage setup shown in Fig. 1(b). Here the iterative map for the longitudinal

Lorentz factor from the nth stage to the $n + 1$th stage for a typical particle[2] is given by

$$\gamma_{n+1} = \gamma_n + \Delta\gamma + \frac{\partial\Delta\gamma}{\partial\psi}\,\delta\psi, \tag{7}$$

where the increase in the Lorentz factor over an acceleration stage is given by

$$\Delta\gamma = \Delta\gamma_{\max}[\sin(\psi_s + \Delta) - \sin\psi_s],$$

with

$$\Delta\gamma_{\max} = 2\gamma_p^2\Phi_0,$$

$$\frac{\partial\Delta\gamma}{\partial\psi} = \Delta\gamma_{\max}[\cos(\psi_s + \Delta) - \cos\psi_s].$$

To the extent that one neglects the order of $\frac{1}{2\gamma_p^2}$, for a typical particle, the deviation of its longitudinal phase from the center of the beam in going from one stage to the next remains fixed; i.e.,

$$\delta\psi_{n+1} = \delta\psi_n = \delta\psi. \tag{8}$$

C. Transverse iterative map

Transverse equation of motion. For the transverse motion of the beam particles in the x direction, we work with the two variables p_x and x. The equations of motion for these two variables are given by the Lorentz force equation and the definition of momentum,

$$\frac{dp_x}{dz} = \frac{dp_x}{cdt} = -\frac{eE_x}{c} \quad \text{and} \quad \frac{dx}{dz} = \frac{p_x}{m\gamma c}. \tag{9}$$

It is shown in Ref. [5] that, in terms of the variable $u = \sqrt{\gamma}x$, the transverse force is approximately harmonic. The two equations of motion lead to

---

[2]Comments on a typical beam particle: Technically we could have introduced beam particle labels, i.e., $i = 1, 2, \ldots, N_0$. Then the ith particle would have a Lorentz factor of $\gamma_i = \gamma_0 + \delta\gamma_i$. Here γ_0 is the Lorentz factor at the "center" of the beam. To be precise, $\delta\gamma_i = \sigma_\gamma\chi_1(i)$ with $\chi_1(i)$ being a random number generated by a Gaussian distribution having a unit width. By the construction here, σ_γ is the Gaussian width, or simply the width, of the variable $\delta\gamma$. For brevity throughout the text we will suppress the beam particle label and refer to, for example, $\gamma = \gamma_0 + \delta\gamma$ as the Lorentz factor for a typical particle which has a width σ_γ. Similarly, the same typical particle will have a longitudinal phase ψ, with a width σ_ψ and a random variable χ_2 from $\{\chi_2(i)\}$. We will also apply the same convention to its transverse coordinates x and x'. They have their widths and the corresponding random variables from the set of $\{\chi_3(i)\}$ and $\{\chi_4(i)\}$.

$$\frac{d^2u}{dz^2} \approx \frac{1}{mc\sqrt{\gamma}}\frac{dp_x}{dz} = -\frac{1}{mc\sqrt{\gamma}}\frac{eE_x}{c} \equiv -\Omega^2 u, \tag{10}$$

where

$$\Omega^2 = \frac{1}{mc\sqrt{\gamma}}\frac{4e}{c\sqrt{\gamma}r_s^2}\frac{\Phi_0 E_{bk}}{k_p}\sin\psi = \frac{\pi a_0^2}{r_s^2\gamma}\sin\psi. \tag{11}$$

Jitters and the transverse map. So far the system is Hamiltonian and thus the emittance of the electron beam is preserved. Now consider jitters in the transverse directions, which, as mentioned earlier, may be due to the misalignment at each stage between the wakefield with respect to the beam line. We follow a procedure similar to those for the generation of random phase space variables. At each acceleration stage a random number χ is generated based on a normalized Gaussian distribution with a width unity. Denote the modified jitter displacement in the x direction by $D = \sqrt{\gamma}\,\sigma_D\chi$. This leads to a following recurrence relation in going from the nth stage to the $n + 1$th stage:

$$\begin{pmatrix} u_{n+1} \\ u'_{n+1} \end{pmatrix} = M_{\text{gap}}M_{wk}\begin{pmatrix} u_n - D \\ u'_n \end{pmatrix} + \begin{pmatrix} D \\ 0 \end{pmatrix}. \tag{12}$$

The wakefield acceleration matrix is given by

$$M_{wk} = \begin{bmatrix} \cos\theta & \frac{1}{\Omega}\sin\theta \\ -\Omega\sin\theta & \cos\theta \end{bmatrix}, \quad \theta = \Omega L_1. \tag{13}$$

Here L_1 is the spatial interval of acceleration, which is the tube length; see Fig. 1(b). From Eq. (6), $L_1 = 2\gamma_p^2\Delta_1/k_p$, where Δ_1 is the phase slip over the corresponding spatial interval. For a gap with a free space interval L_0, the corresponding transport matrix is given by

$$M_{\text{gap}} = S(L) = \begin{bmatrix} 1 & L \\ 0 & 1 \end{bmatrix}. \tag{14}$$

Magnets. It is well known that the presence of magnets increases the stability of electron orbits. Figure 1(c) shows the layout with magnets. Within the gap there is a pair of quadrupoles separated by a distance sL_0, and the distance between each of the magnets to the corresponding end of the tube is given by aL_0. So $2a + s = 1$. With magnets, the matrix M_{gap} is to take on the following form:

$$M_{\text{gap}} \rightarrow S(aL_0)M(f)S(sL_0)M(-f)S(aL_0)$$

$$= \begin{bmatrix} 1 + \frac{s}{b} - \frac{as}{b^2} & [1 - \frac{a^2s}{b^2}]L_0 \\ -\frac{s}{b^2L_0} & 1 - \frac{s}{b} - \frac{as}{b^2} \end{bmatrix}, \tag{15}$$

where $b = f/L_0$ and f is the magnitude of the focal length which is assumed to be the same for both the convergent and the divergent quadrupoles. The magnet matrix in the thin lens approximation, for focal length f, is given by

$$M(f) = \begin{bmatrix} 1 & 0 \\ -\frac{1}{f} & 1 \end{bmatrix}. \tag{16}$$

D. Normalized invariant emittance

Emittance is a measure of the phase space area. A normalized phase space area element is given by

$$\frac{\Delta x \Delta p_x}{mc} = \gamma \Delta x \Delta x' = \Delta u \Delta u', \qquad (17)$$

where we have used $u = \sqrt{\gamma}\, x$, $dx/dt = cx'$, and $p_x = \gamma m \frac{dx}{dt} = \gamma mcx'$. The normalized invariant emittance in the x direction is defined to be the rms value of the phase space area,

$$\epsilon_x = \sqrt{(\sigma_u \sigma_{u'})^2 - c_{uu'}^2} \quad \text{with } c_{uu'} = \langle uu'\rangle - \langle u\rangle\langle u'\rangle, \qquad (18)$$

$$\sigma_u = \sqrt{\langle u^2\rangle - \langle u\rangle^2} \quad \text{and} \quad \sigma_u' = \sqrt{\langle u'^2\rangle - \langle u'\rangle^2}.$$

The emittance of all results shown in this work is for the x phase space.

III. EMITTANCE DEGRADATION AND NUMBER OF STAGES

In this section we will first recall the CTHY model. We will then present our numerical analysis for acceleration with a variable range. Finally, we will consider a simplified version of the CTHY formula based on a stochastic theory consideration, which will serve as a tool for the present emittance degradation analysis.

A. The CTHY model

Plasma. The plasma density $n = 10^{17}$ cm^{-3}. This gives the plasma frequency $\omega_p = [4\pi ne^2/m]^{1/2} = 1.8 \times 10^{13}$ sec^{-1}, the wave number of the plasma waves $k_p = \omega_p/v_p \approx \omega_p/c \approx 6 \times 10^4$ m^{-1}, and the corresponding wavelength $\lambda_p \approx 100$ μm.

Laser. For the laser pulse, the normalized vector potential $a_0 = 0.5$, which gives $\Phi_0 = 0.2$. The laser pulse length is taken to be $L = \lambda_p = 100$ μmm, or 330 fs. We take $\gamma_p = 100$. From Eq. (6), the corresponding laser frequency $\omega = \gamma_p \omega_p = 1.8 \times 10^{15}$ Hz and a wavelength $\lambda = \frac{2\pi c}{\omega} \approx 1$ μm.

Beam. The initial beam energy is taken to be at 0.5 TeV or $\gamma = 10^6$. The percentage energy spread of the initial beam is taken to be 0.01. Longitudinal phase spread $\sigma_\psi = 0.01$ rad.[3] The initial emittance in the x direction at $\epsilon_0 = 2.2$ nm. There is no simple way to determine the average value of the $\sqrt{\sin\psi}$ factor in the betatron frequency, which accounts for the whole quarter-wave region. This average value should be between 0 and 1. Two typical cases were considered by CTHY. For case (a) (see Ref. [3]) this average was taken to be $1/2$, and for case (b) (see Ref. [5]) $\sqrt{2/\pi}$. As we will see later, since in the present work we will be concerned with mainly the small ψ region, we will be comparing our results only with

case (a) of the CTHY model. For this case, the average betatron frequency $\Omega = \sqrt{\Phi_0/\gamma}\,(2/r_s)\sqrt{\sin\psi} = 0.9$ m^{-1}. The corresponding rms radius of the initial beam may be related to the mean betatron frequency in the following way:

$$\epsilon_0 = \Omega\langle u_0^2\rangle = \Omega\gamma\langle x_0^2\rangle \quad \text{or} \quad x_0 = \sqrt{\frac{\epsilon_0}{\gamma\Omega}}. \qquad (19)$$

This leads to $x_0 = 0.05$ μm.

In the CTHY model, the loading phase is fixed at $\psi_s = 0$ rad and the maximum of phase slippage is considered, i.e., $\Delta_{\max} = \psi - \psi_p = \pi/2$. From Eq. (6), the corresponding tube length is given by

$$L_1 = \frac{2\gamma_p^2 \Delta_{\max}}{k_p} = \frac{\pi\gamma_p^2}{k_p} \approx 0.5 \text{ m}. \qquad (20)$$

From Eq. (6) the corresponding energy gain by an electron is given by

$$\Delta\gamma_{\max}mc^2 = 2\gamma_p^2\Phi_0 mc^2 \approx 2 \text{ GeV}. \qquad (21)$$

From initial energy 500 GeV to the final energy of 2.5 TeV, there are 1000 stages. For the case of the jitter parameter $\sigma_D = 0.1$ μm and the initial emittance $\epsilon_0 = 2.2$ nm, the final emittance[4] is $\epsilon \approx 300$ nm $\sim 140\epsilon_0$.

For numerical results in the remainder of this work, all parameters, except those stated otherwise, are the same as those in the CTHY model.

B. Emittance versus total number of stages in a simple multistage model

We are interested in the effect on the emittance degradation due to a reduction in the phase range of acceleration. Since the total acceleration energy is fixed, as the acceleration interval per stage decreases, the number of acceleration stages will accordingly increase. We use the layout of Fig. 1(b) and refer to the system as a "simple multistage model." This is the same as the CTHY model, except that

---

[3]The longitudinal phase spread used in the CTHY model was based on the following considerations. The plasma wavelength is 100 μm. To have a proper acceleration, the longitudinal half-width of the beam σ_z should be less than 10% of the quarter-wavelength acceleration interval. This gives an upper limit, i.e., $\sigma_z \leq 2.5$ μm. In Ref. [6], it is shown that, for such an upper limit, a collider must be operating in the regime where the beam-strahlung parameter Υ is high, and a systematic study of the collider performance in this regime is examined. Based on the criteria of optimizing collider luminosity and to maintain proper longitudinal and transverse beam profiles, it was concluded that $\sigma_z \sim 0.3$ μm, or $\sigma_\psi \sim 0.02$ rad is a reasonable value. Notice the CTHY model value here is a factor of 2 smaller than this quoted value. The CTHY value further helps to keep most of all the beam particles to within the quarter-wave region throughout the entire system.

[4]The value quoted here is for case (a) of the CTHY model. For completeness we also mention that for case (b) of the CTHY model the final emittance is ≈ 700 nm $\sim 320\epsilon_0$.

here we allow the variations of both the tube length and the gap width. Figure 2 shows emittance versus the total number of stages for two sets of gap widths and various jitter parameters at the loading phase $\psi_s = 0.15$ rad. They are given in log-log plots.

There is a general trend that, as the number of stages N increases, the average behavior of emittance decreases persistently. This behavior is to be compared with an inverse-law parametrization

$$\epsilon = \frac{b\sigma_D^2}{N}. \qquad (22)$$

There will be two different b values, one for the gap = 10 tubes cases and one for the gap = tube cases. This parametrization is based on a stochastic theory considered by CTHY and will be discussed in the following subsection. For now it suffices to mention that, to derive this form, among other things one needs to assign a mean betatron frequency, or a mean acceleration phase ψ_m. The approximation which we will be using is given by

$$\psi \approx \psi_m = \psi_s + 0.5\Delta. $$
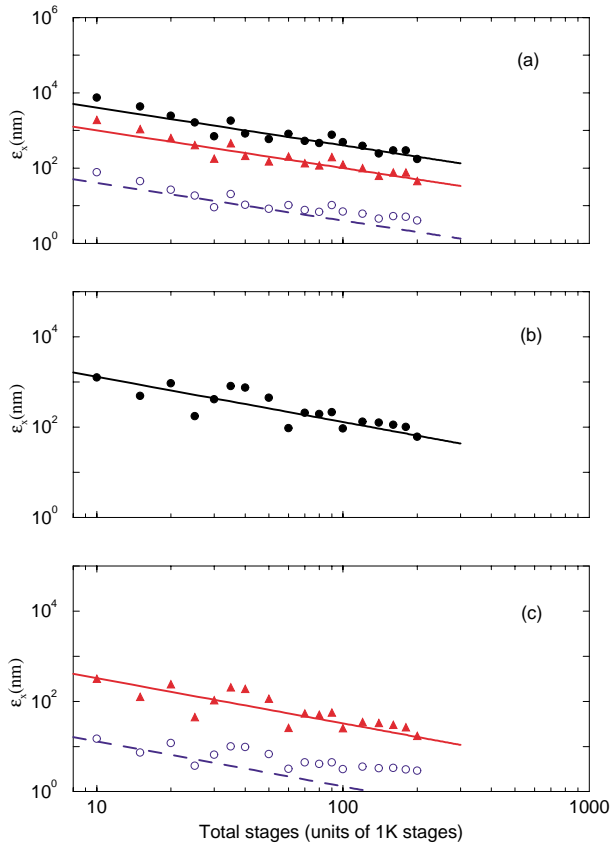
FIG. 2. (Color) Emittance degradation as a function of the total number of stages for two types of gap widths and different jitter parameters: $\sigma_D = 1$ μm (solid circles), 0.5 μm (triangles), and 0.1 μm (open circles). Lines are fits to data points based on a stochastic theory in zero-correlation length approximation. The solid lines are for $\sigma_D = 1$ μm and 0.5 μm, and the dashed lines are for $\sigma_D = 0.1$ μm. (a) gap = 10 tubes, (b),(c) gap = tube.

This approximation is good if Δ is small or the number of stages N is large. We will confine our attention mainly to the region where $\Delta \leq 0.05$ rad or $N \geq 20$.

Figure 2 shows that, for the jitter parameters $\sigma_D = 1$ μm and 0.5 μm, the average rate of fall of data points (solid circles and solid triangles) follows the respective lines reasonably well. There are more pronounced oscillations in the $\sigma_D = 0.5$ μm case as compared to that in the $\sigma_D = 1.0$ μm case.

We now turn to the $\sigma_D = 0.1$ μm cases, where points with open circles are to be compared to the respective dashed lines.

(i) The gap = 10 tubes case is shown in Fig. 2(a). Notice that, in the large N region, e.g., $N \geq 60$ K, the rate of fall of the points is slightly less than that indicated by the dashed line.

(ii) The situation for the gap = tube case is shown in Fig. 2(c). In the large N region the departures of the open circles from the dashed curve in both normalization and slope are very noticeable.

The overall pattern in Fig. 2 suggests the following systematics. The inverse-law parametrization works approximately for large N for those cases where there is a substantial difference (at least 1 order of magnitude) between the relevant emittance and the initial emittance.

C. A stochastic theory for emittance degradation

Using present notations, we proceed to paraphrase some of the stochastic theoretical argument given by CTHY. Here we will mainly confine our attention to the case neglecting the effect of gaps. Toward the end of our discussion we will comment briefly on the situation with the inclusion of gaps. When the cumulative phase of the betatron oscillation per tube θ defined in Eq. (13) is small compared to unity, the transverse equation of motion may be written as follows:

$$u'' + \Omega^2 u = \Omega^2 D = \Omega^2 \sigma_D \chi(z)\sqrt{\gamma} \equiv F(z). \qquad (23)$$

Here we explicitly display the stochastic variable χ which is a random number generated by a Gaussian distribution. Averaging over jitters and in a narrow width approximation, one finds that

$$\langle \chi(z_1)\chi(z_1) \rangle \sim l_c \delta(z_1 - z_2), \qquad (24)$$

where l_c is the correlation length. The solution of this equation is well known (see, for example, [20]). We define the cumulative betatron frequency $\Theta = N\Omega z$, where $z = l_{\text{tube}}$, which measures the distance traversed in the harmonic field within one tube. The second moments are given by

$$\sigma_u^2 = \langle u^2 - \langle u \rangle^2 \rangle = \frac{C}{\Omega^3}\left(\Theta + \frac{1}{2}\sin 2\Theta\right), \qquad (25)$$

$$\sigma_{u'}^2 = \langle u'^2 - \langle u' \rangle^2 \rangle = \frac{C}{\Omega}\left(\Theta - \frac{1}{2}\sin 2\Theta\right), \qquad (26)$$

$$c_{uu'} = \langle (u - \langle u \rangle)(u' - \langle u' \rangle) \rangle = \frac{C}{\Omega^2} \sin^2 \Theta . \qquad (27)$$

Here C is defined through the relationship

$$\langle F(z_1) F(z_2) \rangle = 2C\delta(z_1 - z_2) . \qquad (28)$$

Using Eqs. (23), (24), and (28), one obtains

$$C = \frac{1}{2} \Omega^4 \sigma_D^2 l_c \gamma . \qquad (29)$$

For the final emittance of N multiple stages, the nonoscillatory part of the terms leads to

$$\epsilon \sim \sigma_u \sigma_{u'} \sim \frac{C\Theta}{\Omega^2} \rightarrow \frac{1}{2} [\gamma N l_{\text{tube}} l_c] \Omega^3 \sigma_D^2 . \qquad (30)$$

For a fixed total acceleration energy, $N l_{\text{tube}}$ is constant. Motivated by the data we assume that the correlation length is proportional to the tube length. We denote the proportionality constant by h, which is assumed to depend on the ratio $R = $ gap/tube length. So we obtain

$$\epsilon \propto h(R) \frac{\sigma_D^2 \Omega^3}{N} \propto h(R) \frac{\sigma_D^2 \sin^{3/2} \psi}{N} . \qquad (31)$$

For the last step we recall the definition of Ω given in Eq. (11). The $(\sin^{3/2} \psi)$ behavior will play an important role in our discussion.

Now we come to the case with gaps. It turns out that in a small phase angle approximation, i.e., the angles of rotation in the transverse phase space associated with the travel within a tube and within a gap are assumed to be small, one finds that Eq. (31) can be generalized to[5]:

$$\epsilon \rightarrow \sqrt{l_{\text{tube}} + L} \frac{\sigma_D^2 \Omega^3}{N} , \quad \text{thus } h(R) = \sqrt{\frac{l_{\text{tube}} + L}{l_{\text{tube}}}} .$$

Let us come back to Fig. 2. Working with the conventional units of expressing σ_D in units of μm and ϵ in units of nm, from fits shown in Fig. 2 the coefficient of Eq. (22) for the gap = 10 tubes case is given by $b = 4 \times 10^4$ and that for the gap = 1 tube case by $b = 1.3 \times 10^4$. This leads to the ratio $h(10)/h(1) \approx 3$. The CTHY stochastic model gives $\frac{h(10)}{h(1)} \approx \sqrt{11/2} \sim 2.3$, which is in the same ballpark.

----

[5]Denote the resultant transfer matrix from the nth state to the $n + 1$th state by M, which transports beam particles through one tube and one gap. It can be shown that the inverse of the effective betatron frequency can be written as $\frac{1}{\Omega_{\text{eff}}} = \frac{M_{12}}{\sin \sigma}$, where $\cos \sigma = \frac{\text{Tr} M}{2}$. In the small phase angle approximation assumed, i.e., Ωl_{tube} and $\Omega L \ll 1$, after some algebra one obtains $\Omega_{\text{eff}} \approx \Omega \sqrt{l_{\text{tube}}/(l_{\text{tube}} + L)}$. Taking into account that the effective rotating phase associated with the passage of one tube and one gap is given by $\Omega_{\text{eff}}(l_{\text{tube}} + L)$, one finds $\epsilon \rightarrow \frac{1}{2} [\gamma N (l_{\text{tube}} + L)^2] \Omega_{\text{eff}}^3 \sigma_D^2 \propto \sqrt{l_{\text{tube}} + L} (\sigma_D^2 \Omega^3 / N)$.

IV. APPROXIMATELY SYNCHRONOUS ACCELERATION

In this section we consider an approximately synchronous acceleration model with superunits and chips, or the chip model. We will begin with the general layout of the model and then turn to numerical results.

A. Accelerator with superunits, chips, and magnets

With the scenario of having a very large number of stages, each stage becoming very short (e.g., of the order of 1 cm), we are led to consider a superunit which is made out of many short tubes, or chips, as depicted in Fig. 3(a). Here wakefield within each chip is created by an independent laser pulse. The stochastic jitters are contributed by, among other things, the misalignment between each pulse and the beam line characterized by a Gaussian width σ_D, referred to as the jitter parameter or the offset parameter [see comments leading to Eq. (12)]. We allow for the order of 1 m between adjacent superunits to allow the experimental set up needed to maintain superunits including magnets placed over a certain period of length to maintain the quality of the beam. We consider a mixed configuration, where there are superunits. Within each superunit, there are many short tubes closely spaced and interspersed by large gaps [see Fig. 3(b)]. We have considered an illustrative system: the total energy is 2.5 TeV, which is used as each of the two arms of the 5 TeV collider, and the acceleration is from 0.5 to 2.5 TeV; the total number of superunits (SU) is 500; within one superunit there are 100 stages per SU and gap = tube = 0.83 cm; there is a large (1 m) gap between two adjacent superunits; the length of the accelerator is about 1300 m.

B. Emittance degradation as a function of loading phase

We proceed to look at how emittance degradation varies as a function of the loading phase for the system of superunits with chips. From Eq. (31), one expects in some average sense

$$\epsilon \propto \langle \Omega^3 \rangle \propto (\sin \psi_m)^{3/2}, \qquad (32)$$

a. Super Unit with chips

b. Accelerator Layout
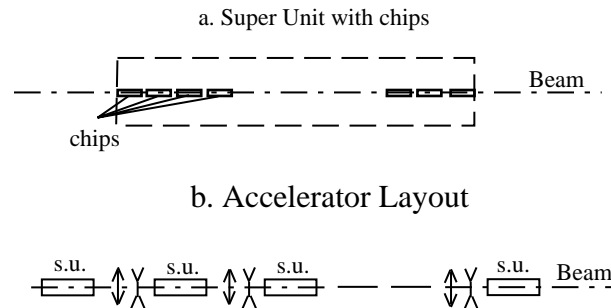
FIG. 3. Chip model. (a) A superunit with chips and (b) the chip model accelerator layout.
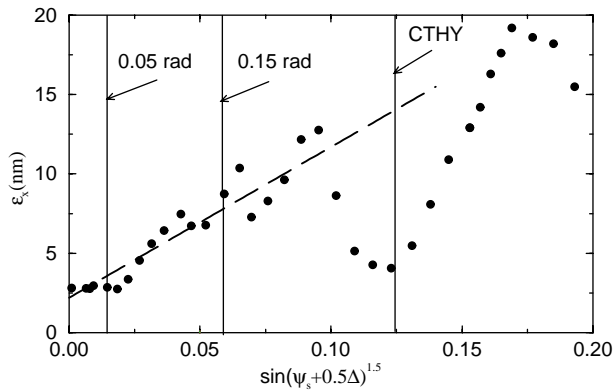
FIG. 4. A comparison between data points based on the chip model with $\sigma_D = 0.1$ μm and the $\sin^{3/2}\psi$ law as indicated by the dashed line.

where ψ_m is the mean phase of the beam; as mentioned earlier we take it to be $\psi_m = \psi_s + 0.5\Delta$. Here ψ_s is the loading phase and Δ is the total phase slip. Figure 4 shows the final emittance as a function of $(\sin\psi_m)^{3/2}$ at the default value $\sigma_D = 0.1$ μm. In the small ψ_m region up to $(\sin\psi_m)^{3/2} \sim 0.1$ the emittance degradation has an approximately linear behavior superposed by a small oscillation. Beyond this point, the oscillatory behavior becomes violent.

This implies that the resilience of the present system against jitters can be further improved, at least in the small loading phase region, by lowering the loading phase value. With this in mind, we will also consider two loading phases, i.e., $\psi_s = 0.15$ and 0.05 rad.

C. Different loading phases and magnets

Figure 5 shows the interim emittance degradation for three cases. They are all at the final energy 2.5 TeV.

Case (a), 50 K stages, $\psi_s = 0.15$ rad. The final emittance $\epsilon = 7.3$ nm $= 3.3\epsilon_0$. (As mentioned in Sec. III A, throughout this work the initial emittance is assumed to be $\epsilon_0 = 2.2$ nm.)

Case (b), 50 K stages, $\psi_s = 0.05$ rad. The final emittance $\epsilon = 2.85$ nm $= 1.3\epsilon_0$. One sees that the qualitative expectation of the $(\sin\psi)^{3/2}$ law is satisfied here.

Case (c), 20 K stages, $\psi_s = 0.15$ rad. The final emittance $\epsilon = 10.3$ nm $= 4.7\epsilon_0$

Notice that case (a) is for 50 K and case (c) is for 20 K. Both are at the final energy 2.5 TeV. As expected, the final emittance for the 20 K case is greater than that for the 50 K case.

The stochastic theory, if applicable, implies that the intermediate emittance should grow approximately[6] linearly with the number of stages; see Eq. (30). Approximate
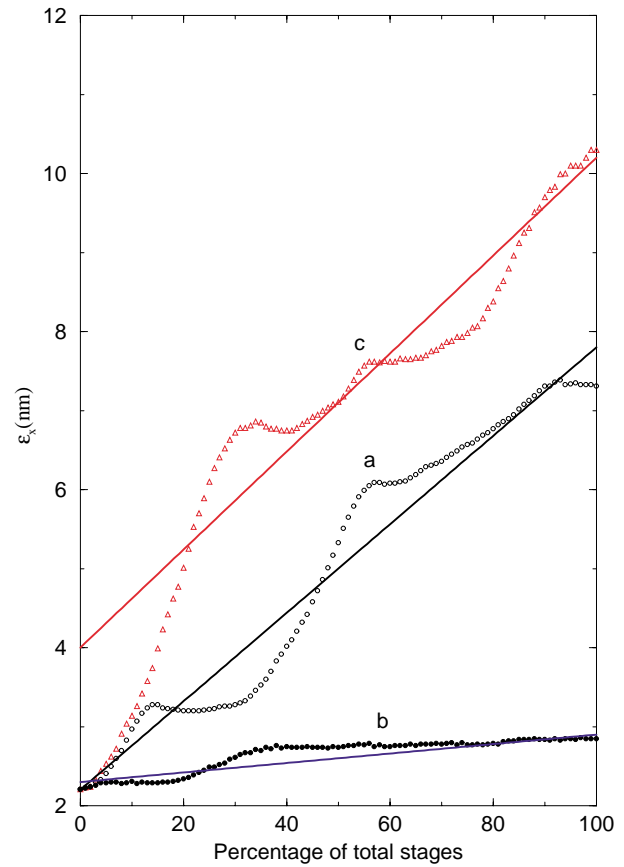
FIG. 5. (Color) The interim emittance degradation behavior as the beam particles traverse through the system of a chip model for $\sigma_D = 0.1$ μm. For each case, a solid line of a linear behavior is included to guide the eye. Curve a, total stages 50 K, $\psi_s = 0.15$ rad. Curve b, total stages 50 K, $\psi_s = 0.05$ rad. Curve c, total stages 20 K, $\psi_s = 0.15$ rad.

mean linear behavior is observed for curves (a) and (b). For curve (c), there is a rapid rise up to about 20% of the total stages, which is followed by an approximately linear mean behavior.

In our previous investigation in Ref. [10], the effect of magnets was considered. The setup for the simple multistage system and that for the system with the superunits with chips are identical to those cases considered in the present work, except for one difference. The final energy there is at 3 TeV, which is to be compared to 2.5 TeV for the present case.[7]

We mention several points on this 3 TeV work. For the simple multistage model the inverse-power law worked in a similar manner as that presented in this work. For the chip model, with the jitter parameter $\sigma_D = 0.01$ μm, and the loading phase 0.15 rad, the final emittance is 10.4 nm. (This is to be compared to 7.3 nm for the present case.)

---

[6]It is shown in Ref. [5] that if the tube length is fixed and total energy is allowed to vary, for very large N, the emittance grows as $\sqrt{N}\ln N$.

[7]There is a misprint in the energy label of our previous work given in [10]. The final energy of each of the accelerators should be 3 TeV, not 2.5 TeV.
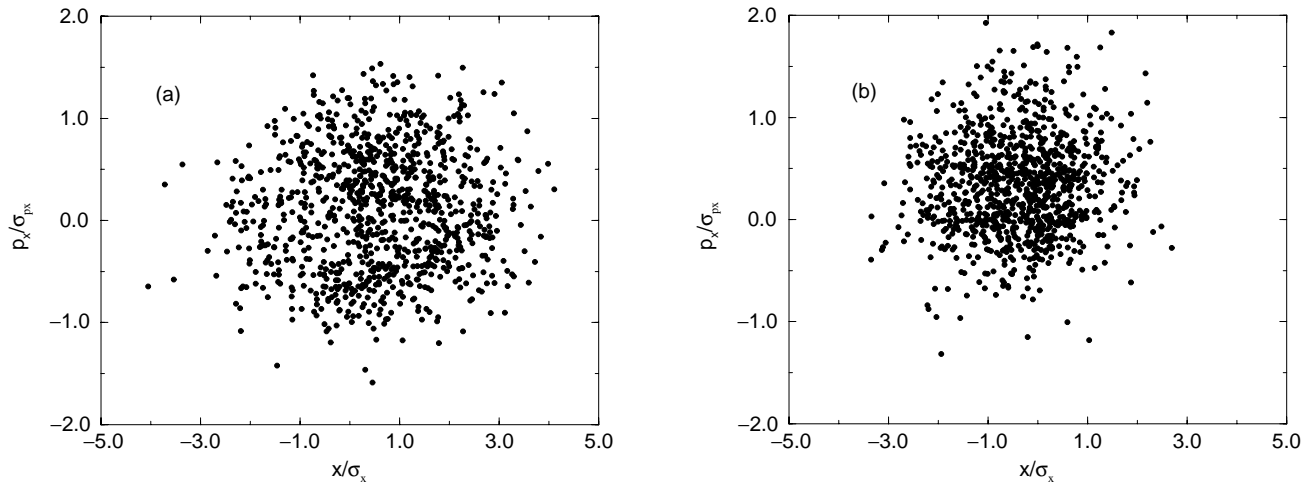
FIG. 6.   Traverse phase space: normalized p_x versus normalized x, for $\psi_s = 0.15$ rad. The final average beam energy is at 3 TeV (see text). (a) Without magnets and (b) with magnets.

When the magnets were included, the final emittance was lowered from 10.4 to 6.6 nm. The effect of magnets can be seen visually in the transverse phase space plot. This is shown in Fig. 6.

We return to the present 2.5 TeV model. Figures 4 and 5 are for the jitter parameter, $\sigma_D = 0.1$ μm. We digress here to show in Fig. 7 the emittance degradation
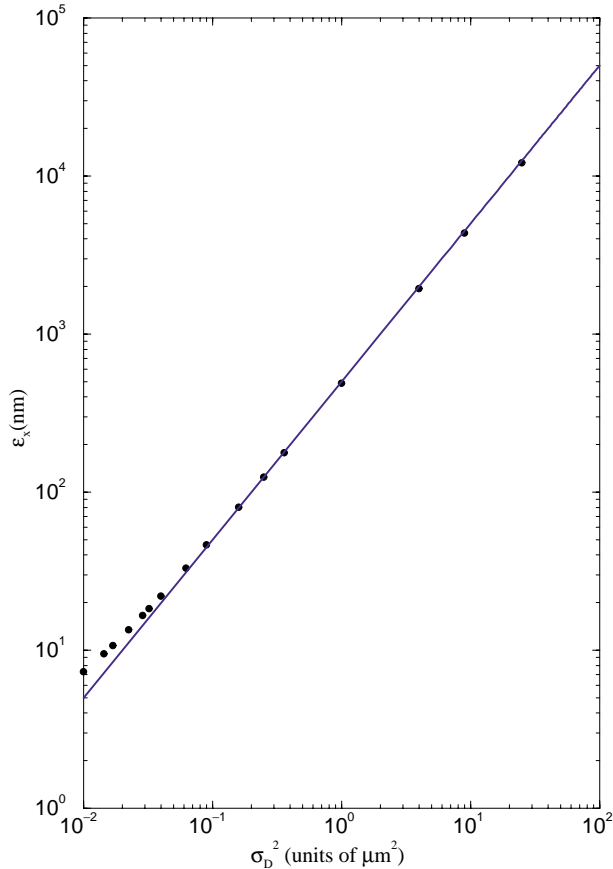
FIG. 7. (Color) Emittance degradation versus σ_D^2. A fit to the linear behavior is given to guide the eye [see Eq. (31)].

as a function of σ_D^2 for the case where the loading phase is at 0.15 rad. It is a log-log plot. It shows that the emittance is, as expected from Eq. (31), to grow asymptotically with σ_D^2. It also illustrates that the jitter parameter used for the three cases considered here, $\sigma_D^2 = (0.1 \ \mu\text{m})^2$, is below the threshold of the linear region. The onset of the σ_D^2 behavior occurs near $\sigma_D^2 = (0.2 \ \mu\text{m})^2$.

To conclude, within the present chip model the final emittance has been reduced to, say, less than $2\epsilon_0$, this is to be compared to the situation in the CTHY model, where the final emittance is beyond $100\epsilon_0$. This, however, is at the expense of introducing 50 times more laser pulses; in turn the power consumption is also increased by many fold. Thus it has severe practical limitations. These limitations might be ameliorated by adopting a technique to flip a phase by π by introducing two counterpropagating lasers with slightly different colors (Shvets' method [21]).

V. SYNCHRONOUS ACCELERATION

A. Horn model

As mentioned earlier, synchronous acceleration may be achieved through a specific variation of the plasma density. In this section we will first demonstrate that, in general, a smoothly varying density profile may be achieved through the appropriate variation of the local cross section area of the tube. We will then derive the analytic expressions for the longitudinal and transverse maps for the synchronous acceleration. Last, we will present our numerical results

A steady flow picture and the horn model. Consider a steady adiabatic flow of a fluid from a reservoir through a nozzle, say, in the z direction. Let the static fluid density of the fluid in the reservoir be ρ_0, which will be referred to as the quiescent density. Denote the fluid density at z along the nozzle as $\rho(z)$. In the Appendix we will show that, based on fluid dynamics [16], the following relation is valid:

$$A(z) = \text{const} \times \left(\frac{\rho(z)}{\rho_0}\right)\sqrt{1 - \left(\frac{\rho(z)}{\rho_0}\right)^{\gamma-1}}, \quad (33)$$

where γ is the usual ratio of the specific heat at a constant pressure to that at a constant volume. For a monotonic gas $\gamma = 5/2$, and for a diatomic gas $\gamma = 7/2$. Figure 8 shows the plot of $A/A_{\min}$ versus $\rho(z)/\rho_0$ for $\gamma = 5/2$ (solid circles) and also that for $\gamma = 7/2$ (solid line). Here $A_{\min}$ is the minimum cross sectional area of the nozzle, which takes on a different value for each case. For each curve, the appropriate domain of present interest is to the right of the minimum point. In this region, the density increases with the cross section, which corresponds to the subsonic region of the fluid flow. There is a one-to-one relationship between the cross sectional area A and the plasma density ρ. By increasing the cross section along the beam direction in a specified way, one may achieve the required density function. Looking down the stream of the beam, the accelerator consists of a system of aligned horns, although in some cases the increase in radius may be slight. This is why we refer to the present model as the "horn model." Figure 9(a) is a schematic illustration of the layout of this model.

Density function and $\zeta(z)$. Now we come to Katsouleas's [15] matching condition. Consider the wakefield acceleration of a beam electron which is located at the center of the beam. Let the "loading number" N_{load} be the number of wave crests where the electron is lagging behind the laser pulse. If the initial electron phase relative to the local wakefield, as defined earlier, is ψ_s, then the electron phase relative to the laser pulse defined by the local plasma wave number k_p is

$$k_p s_1 = 2\pi N_{\text{load}} - \psi_s,$$

where s_1 is the distance from the electron to the pulse measured in the rest frame of the pulse.

To motivate for the matching condition, for the time being imagine the horn has been divided into many segments. For now we work with a finite number of segments. We will assume the density is constant within each segment. For the ith and the $i + 1$th segments, the wave numbers are k_{pi} and k_{pi+1} respectively. Here the approximate synchronous condition is to have the electron phase relative to the laser pulse be the same at the start of each segment. We will derive this approximate synchronous condition through an inductive reasoning. Assume this condition is already satisfied up to the beginning of the ith segment. The ith segment has a width Δz and has a phase slip of $\Delta\psi$. Let the distance between the laser pulse and the electron at the of end of the ith segment be s_1. Here its phase measured by the wave number of the ith segment is $k_{pi}s_1 = 2\pi N_{\text{load}} - \psi_s - \Delta\psi$. The synchronous condition requires the recovery of the initial phase at the start of the $i + 1$th segment, i.e., $k_{pi+1}s_1 = 2\pi N_{\text{load}} - \psi_s$. In other words, the matching condition is given by

$$\frac{2\pi N_{\text{load}} - \psi_s - \Delta\psi}{k_{pi}} = \frac{2\pi N_{load} - \psi_s}{k_{pi+1}}. \quad (34)$$

Figure 9(b) shows the situation for the case where $\psi_s = 0$. We write $k_{pi+1} = k_{pi} + \frac{dk}{dz}\Delta z$, where Δz is the width of the ith segment. In the continuum limit, after some algebra it leads to

$$\frac{1}{k_p}\frac{dk_p}{dz} = \frac{1}{2\pi N_{\text{load}} - \psi_s}\frac{d\psi}{dz}$$

$$= \frac{1}{2(2\pi N_{\text{load}} - \psi_s)c}\frac{\omega_p^3}{\omega_0^2}. \quad (35)$$

FIG. 8. (Color) Relationship between the normalized cross section and the normalized density function in a nozzle flow. The solid circles are for the monoatomic plasma and the curve is for the diatomic plasma.

a. Horn Model

b. Synchronous Condition

$$s_1 = \frac{2\pi N_{\text{load}} - \Delta\phi}{k_i} = \frac{2\pi N_{\text{load}}}{k_{i+1}}$$
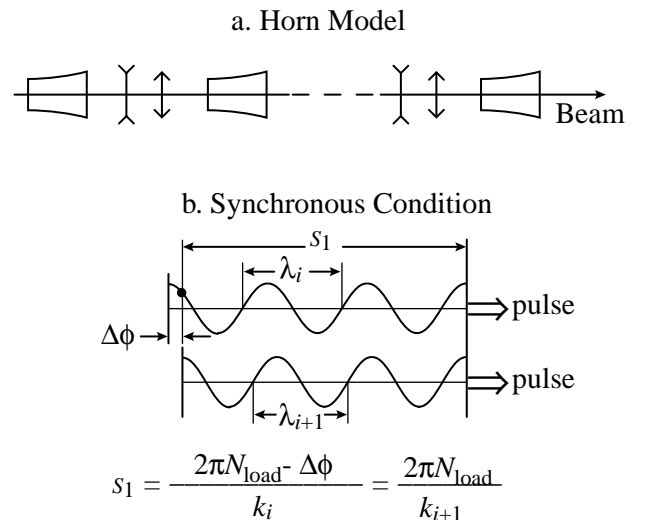
FIG. 9. The horn model. (a) Matching condition for synchronous acceleration for the case where $\psi_s = 0$. (b) A schematic layout of the horn model.

Here ω_0 is the frequency of the laser pulse. In the last step, Eq. (6) and $k_p = \omega_p/c$ were used. The first equality is the Katsouleas condition for synchronous acceleration.

To proceed to evaluate the number density variation within the horn, we first recall that the frequency of plasma waves is proportional to the square root of the number density. Thus the z dependence of all three quantities, the number density of the plasma medium, the frequency, and the wave number of plasma waves, may be specified by a single z-dependent function $\zeta(z)$. In particular, one may write

$$n(z) = n_0\zeta(z)^2, \qquad \omega_p(z) = \omega_{p0}\zeta(z),$$
$$k_p(z) = k_{p0}\zeta(z). \tag{36}$$

Substituting Eq. (36) into Eq. (35) gives

$$\frac{1}{k}\frac{dk}{dz} = \frac{1}{\zeta}\frac{d\zeta}{dz} = \frac{1}{2(2\pi N_{\text{load}} - \psi_s)c}\frac{\omega_{p0}^3}{\omega_0^2}\zeta^3, \tag{37}$$

To the extent one neglects the pump-depletion effect [17], i.e., the loss of laser pulse energy as it traverses through the horn, the intensity and the frequency of the laser pulse is assumed to be a constant. Integrating over Eq. (37) leads to

$$\zeta(z) = \frac{1}{(1 - z/z_0)^{1/3}},$$
$$z_0 = \frac{2(2\pi N_{\text{load}} - \psi_s)c}{3}\frac{\omega_0^2}{\omega_{p0}^3}. \tag{38}$$

Constraint due to conservation of energy. We turn to the correction due to the pump-depletion effect. During the acceleration process, there is an energy transfer from the laser pulse to the wakefield created. Again we will first consider the situation with finite segments then take the continuum limit.

From the relationship between E and the vector potential A, $E = -\partial A/\partial ct$, and Eq. (1), the electric field amplitude of the laser pulse with a frequency ω is given by

$$E_l = \omega a\left(\frac{mc}{e}\right), \tag{39}$$

where a is the normalized vector potential. From Eq. (3), the wakefield created by the pulse is given by

$$E_w = \frac{\pi\omega_p}{4}a^2\left(\frac{mc}{e}\right). \tag{40}$$

Denote the length of the laser pulse by L_l. Assume the cross section of the laser pulse and that of the wakefield are the same. Both are labeled as A. Some portion of the energy of the laser pulse goes into the creation of the wakefield in the ith segment and the remainder enters into the $i + 1$th segment. So there is the relation

$$AL_lE_{li+1}^2 = AL_lE_{li}^2 - A\Delta zE_{wi}^2, \tag{41}$$

where Δz is the width of the ith segment. Denote the normalized vector potential of the laser pulse at the ith

element by a_i. Making use of the above equations, it leads to the recursion relation

$$(\omega a)_{i+1}^2 = (\omega a)_i^2 - \frac{\Delta z}{L_l}\left(\frac{\pi}{4}\omega_{pi}\right)^2 a_i^4. \tag{42}$$

Here ω_{pi} is related to the plasma density n_i, which will be determined by a matching condition to be given below.

Constraint due to adiabatic invariance. We assume that the wakefield creation is an adiabatically invariant process. As the energy of the laser pulse decreases, the average frequency of a laser pulse should also be decreasing according to the relation (see, for example, [18])

$$\omega_i = \omega_0\left(\frac{a_i}{a_0}\right)^2. \tag{43}$$

Substituting this relation into the above recursion relation and after some algebra, one arrives at

$$\left(\frac{\omega_0^2}{a_0^4}\right)a_{i+1}^6 = \left(\frac{\omega_0^2}{a_0^4}\right)a_i^6 - \frac{\Delta z}{L_l}\left(\frac{\pi}{4}\omega_p\right)^2 a_i^4. \tag{44}$$

Writing $\Delta a^6 = a_{i+1}^6 - a_i^6$, in the continuum limit, the recursion relation Eq. (44) now becomes

$$\frac{1}{a^4}\frac{da^6}{dz} = -\left[\frac{a_0^4}{\omega_0^2}\left(\frac{\pi}{4}\omega_p\right)^2\right]\frac{1}{L_l} = -\frac{a_0^2\zeta^2(z)}{D},$$
$$D = \left(\frac{4}{\pi a_0}\frac{\omega_0}{\omega_{p0}}\right)^2 L_l. \tag{45}$$

Integrating both sides, one obtains

$$\xi(z) \equiv \left(\frac{a}{a_0}\right)^2 = 1 - \frac{z_0}{D}\left[1 - (1 - z/z_0)^{1/3}\right]. \tag{46}$$

Acceleration energy and the $\eta(z)$ function. From Eq. (38), $k_p = k_{p0}\zeta(z)$ and $\Phi_0 = \Phi_0(0)\xi(z)$, the acceleration energy is given by

$$\Delta\gamma(z) = \int_\gamma^{\gamma(z)}d\gamma = \int_0^z k_p\Phi_0\cos\psi\,dz$$
$$= \cos\psi\int_0^z k_{p0}\Phi_0(0)\xi(z)\zeta(z)\,dz$$
$$= \Delta\gamma_{\max}\cos\psi\,\eta(z). \tag{47}$$

Taking z_1 to be the length of the horn, we obtain

$$\Delta\gamma_{\max} = k_{p0}\Phi_0(0)z_1,$$
$$\eta(z) = \frac{3z_0}{z_1}\left\{\left(1 - \frac{z_0}{D}\right)\left[1 - (1 - z/z_0)^{2/3}\right] + \frac{2z}{3D}\right\}. \tag{48}$$

Cumulative phase and $\langle\xi^{1/2}\rangle$. The cumulative phase in the transverse direction for a typical particle[8] is given by

---

[8]We remind the reader that our "typical particle" convention was discussed in Footnote 2. For brevity we will continue to suppress particle labels for γ and ψ and in turn also for those quantities which are expressed in terms of them.

$$\theta = \int \Omega(z') \, dz' = \int_0^z \left[\frac{\pi \sin\psi a^2(z')}{r_s^2 \gamma(z)} \right]^{1/2} dz'$$

$$\approx \Omega_m z_1 \langle \xi^{1/2} \rangle. \tag{49}$$

Here we have approximated the z-dependent γ factor in the integrand by the midpoint value γ_m and write

$$\Omega_m = \left[\frac{\pi \sin\psi a_0^2}{r_s^2 \gamma_m} \right]^{1/2}. \tag{50}$$

The average value

$$\langle \xi^{1/2} \rangle = \frac{1}{z_1} \int_0^{z_1} \xi^{1/2}(z) = \frac{3}{b^3} \left(\frac{z_0}{z_1} \right) \sqrt{1 - \frac{z_0}{D}} \, F(b,x), \tag{51}$$

$$b = \frac{z_0}{D - z_0} \quad \text{and} \quad x = b \left(1 - \frac{z_1}{z_0} \right)^{1/3},$$

and

$$F(b,x) = [f_1(b) - f_1(x)] - [f_2(b) - f_2(x)] + [f_3(b) - f_3(x)], \tag{52}$$

where

$$f_1 = \frac{2}{3} x(1 + x)^{3/2}, \qquad f_2 = \frac{2^3}{3 \times 5} x(1 + x)^{5/2}, \tag{53}$$

$$f_3 = \frac{2^4}{3 \times 5 \times 7} x(1 + x)^{7/2}.$$

Iterative maps. To sum up, the longitudinal map from the nth stage to the $n + 1$th stage for a typical particle is given by

$$\gamma_{n+1} = \gamma_n + \Delta\gamma(z_1) + \frac{\partial \Delta\gamma}{\partial \psi},$$

$$\frac{\partial \Delta\gamma}{\partial \psi} = -\tan\psi_s \Delta\gamma(z_1) \delta\psi. \tag{54}$$

The spread of the phase of a typical particle $\delta\psi$ is again assumed to be approximately constant throughout the entire acceleration stages. The transverse map has the same form as that given in Eqs. (12) and (13), with θ defined by Eq. (49) and the corresponding betatron frequency Ω_m evaluated at the midpoint of the horn, which is given by Eq. (50).

B. Numerical results

For the present synchronous acceleration case, there is no quarter-wavelength restriction, so the tube length can *a priori* vary over a range of values.

Figure 10 shows the emittance degradation for the tube length ranging from 0.2 to 1.4 m, keeping the gap width at the nominal value of 1 m. We recall that, in the CTHY model, there is a full-quarter-wavelength acceleration, the tube length is 0.5 m. For the present model, Fig. 10 indicates that the tube length less than 0.4 m is preferred. For our calculation below, we fix the tube length to be at 0.35 m.
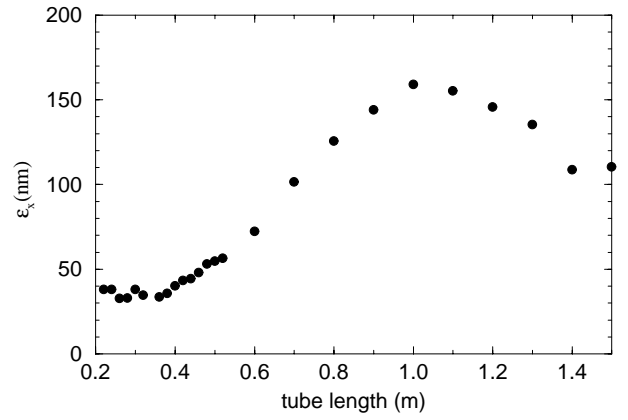
FIG. 10.   Emittance degradation as a function of the tube length, where the gap is kept fixed at 1 m.

Table I gives the normalized final densities and the acceleration energies and other items for loading numbers N_{load} ranging from 1 to 5. One sees that both the final density (normalized to ρ_0) and the acceleration energy are not sensitive to the loading number. We have also verified that the emittance degradation is also not too sensitive to the loading number. For all figures presented in this section, the loading number has been set to 5. For these cases, from Table I we see that the density variation per horn is 7%, with the acceleration energy per stage 2.08 GeV, which is comparable to that of the CTHY model.

The value of the betatron frequency depends on the beam energy. As the beam being accelerated, the betatron frequency will decrease. So the betatron frequency has its largest value initially. For the present case, using the expression in Sec. III A the initial betatron value for the loading phase of 0.04 rad is given by $\Omega = 0.35 \text{ m}^{-1}$. With the tube length of 0.35 m, the cumulative betatron oscillation phase per horn is 0.12 rad, which is small compared to $\pi/2 \sim 1.6$ rad. The total cumulative phase over the entire accelerator system, which consists of about 960 stages, is $\Theta \sim 120$ rad. The spread in Θ is given by

$$\delta\Theta = N\delta\Omega l_{\text{tube}} \sim \frac{1}{2} \left[\left(\frac{\delta\psi}{\psi} \right)^2 + \left(\frac{\delta\gamma}{\gamma} \right)^2 \right]^{1/2} \Theta, \tag{55}$$

with $\delta\psi$ and $\delta\gamma$ being the spread in ψ and that in the Lorentz factor, respectively. For a fixed $\delta\psi$, the smaller

TABLE I.   Horn model: tube length = 0.35 m.

N_{load}	Normalized final density	Acc. energy (GeV)	$z_0(m)$	ξ	η
1	1.60	2.26	0.70	0.92	1.10
2	1.21	2.14	1.39	0.85	1.04
3	1.13	2.10	2.09	0.78	1.02
4	1.09	2.08	2.79	0.71	1.01
5	1.07	2.08	3.49	0.64	1.01
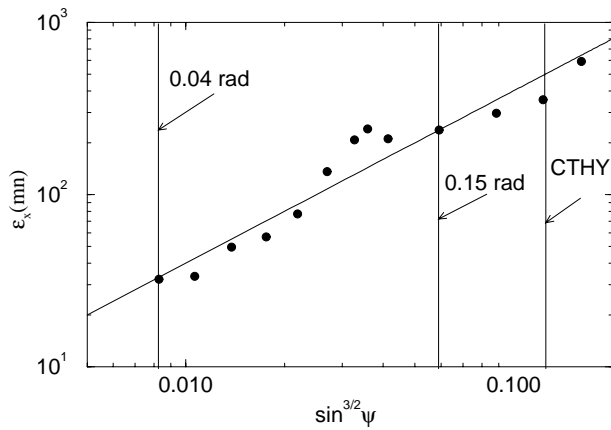
FIG. 11. A comparison between the $\sin^{3/2}\psi$ law, indicated by the line, and the data for the horn model.

the acceleration phase, the larger the value of $\delta\Theta$. Using $\delta\gamma/\gamma = 0.01$ and $\delta\psi = 0.01$, for case (a) where the loading phase is 0.04 rad, the cumulative spread $\delta\Theta$ is about 15 rad. Thus the phase space has already reached a full mixing state. For the loading phase 0.15 rad, the corresponding spread $\delta\Theta$ is about 4, the phase space is about two-thirds of the way toward a full mixing state. For case (a) where $\psi_s = 0.04$, the full mixing stage has
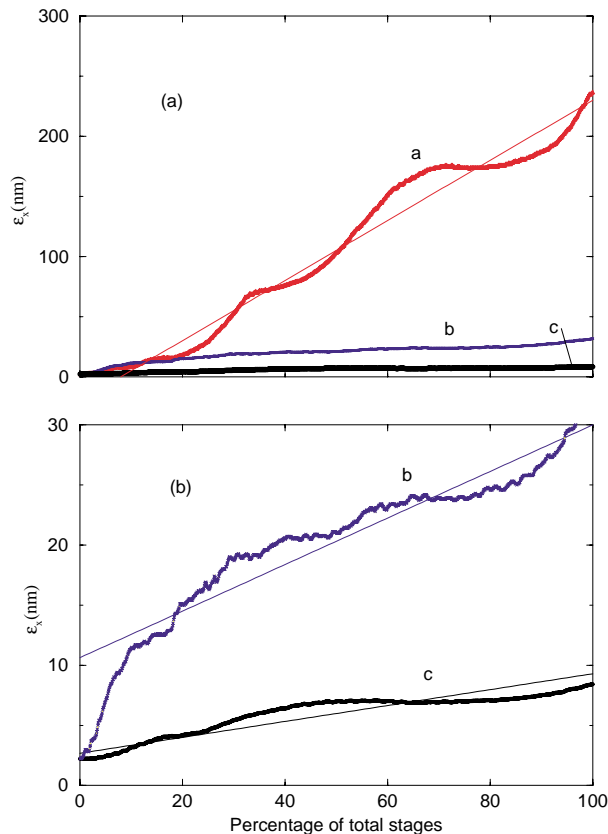
FIG. 12. (Color) The emittance degradation for three cases of the horn model. Curve (a), $\psi = 0.15$ rad. Curve (b), $\psi = 0.04$ rad. Curve (c), $\psi = 0.04$ rad and $d\psi = 0.0001$ rad.
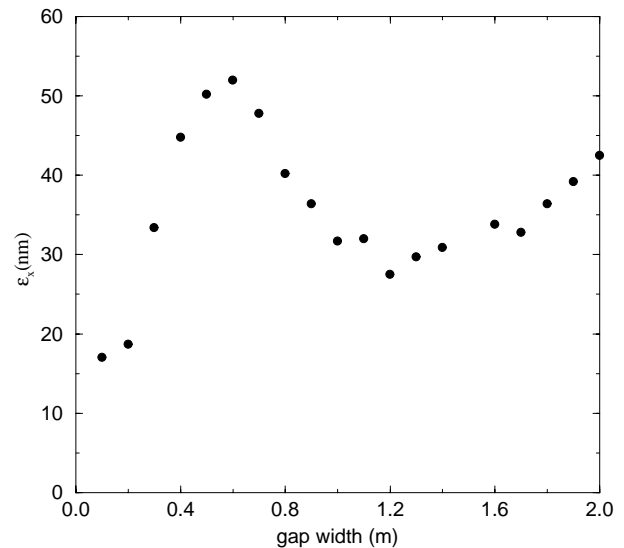
FIG. 13. Gap width dependence of the emittance degradation.

already occurred, and, for the case where $\psi_s = 0.15$, the phase space is about to reach a full mixing state.

Figure 11 shows the plot of emittance degradation versus $(\sin\psi)^{3/2}$. Here it is a log-log plot. The line has a unit slope. It illustrates that the $(\sin\psi)^{3/2}$ law is operative here.

In Fig. 12, curve (a) corresponds to the case where $\psi_s = 0.15$ rad. Here the final emittance is $\epsilon = 237$ nm $\sim 108\epsilon_0$, which is in the same ballpark as that of the CTHY model, which is $\sim 140\epsilon_0$. So far we have not gained much ground. The important case is curve (b), which is the case where $\psi_s = 0.04$ rad. It has a final emittance $\epsilon = 31.7$ nm $\sim 14.5\epsilon_0$, which is about 1 order of magnitude reduction as compared to that of the CTHY model. The interim emittance for this case is shown in Fig. 12(a) and with an amplified scale in Fig. 12(b).

The emittance degradation is sensitive to the longitudinal phase spread of the beam which for all cases considered up to now has been taken to be $\sigma_\psi = 0.01$ rad. Curve (c) illustrates the case for a negligibly small value of the spread, i.e., $\sigma_\psi = 0.0001$ rad. Here the final emittance is given by $\epsilon = 8.4$ nm $\sim 3.8\epsilon_0$.

So far the gap width is fixed at 1 m. Figure 13 shows the situation where the tube length is kept at 0.35 m but the gap width is allowed to vary. Notice as long as the gap width is of the order of 1 m , ranging, say, from 0.8 to 2 m, the emittance degradation is not sensitive to variation of the gap width.

VI. SUMMARY AND DISCUSSION

We have been looking for ways to suppress emittance degradation in multistage wakefield accelerator systems at a fixed final energy, 2.5 TeV. In the course of our analysis, we have paid special attention to three quantities: the total number of stages N, the phase angle of acceleration ψ, and the jitter parameters σ_D. The values of all other parameters are kept fixed as those given in the CTHY model. From a

TABLE II.   Laser-wakefield accelerator models: 2.5 TeV, $\sigma_D = 0.1$ μm.

Index	Model	ψ_m	N	ϵ	ϵ^{pred}	R_{ij}
CTHY	CTHY	0.25 rad	1 K	$140\epsilon_0$	$231\epsilon_0$	$R_{03} = 2.15$
1	chip	0.16 rad	50 K	$3.3\epsilon_0$	$3.2\epsilon_0$	$R_{13} = 0.021$
2	chip	0.06 rad	50 K	$1.3\epsilon_0$	$1.5\epsilon_0$	$R_{21} = 0.23$
3	horn	0.15 rad	0.96 K	$108\epsilon_0$	$108\epsilon_0$	$R_{33} = 1.0$
4	horn	0.04 rad	0.96 K	$14.5\epsilon_0$	$16.0\epsilon_0$	$R_{43} = 0.14$

stochastic theory considered by CTHY, emittance growth in terms of these parameters is given by

$$\Delta\epsilon = \epsilon_f - \epsilon_0 \propto \frac{(\sin\psi_m)^{3/2}\sigma_D^2}{N}. \quad (56)$$

Figure 7 is an example which illustrates that the quadratic power dependence of the jitter parameter is well satisfied for large (asymptotic) values of the parameter. This asymptotic behavior turns out to be universal for all cases considered, although the locations for the onset of the asymptotic behavior do vary from case to case.

How general is Eq. (56)? To our pleasant surprise we have found that at least within restricted parameter ranges it works reasonably well. It works not only "internally," i.e., within a given model, e.g., within the chip model and within the horn model. It also works "externally," i.e., among all three models: the chip, the horn, and the CTHY models. In Table II we list the final emittance for five relevant cases, where the jitter parameter is fixed at $\sigma_D = 0.01$ μm. What we would like to show is how well, based on a given reference emittance of, say, case j, ϵ_j, one can predict the final emittance of case i, ϵ_i^{pred}, for various values of i. One can make such prediction through the relationship

$$\epsilon_i^{\text{pred}} = R_{ij}(\epsilon_j - \epsilon_0) + \epsilon_0, \quad (57)$$

where

$$R_{ij} = \left(\frac{\sin\psi_{mi}}{\sin\psi_{mj}}\right)^{3/2}\left(\frac{N_j}{N_i}\right).$$

To minimize uncertainties we will begin with case (c), which has the largest emittance among the chip and the horn models. Case (c) is for the horn model with 960 stages and $\psi = 0.15$ rad. By tautology, $R_{33} = 1$, and the "predicted" final emittance for this case is $\epsilon_3^{\text{pred}} = \epsilon_3 = 108\epsilon_0$. It is listed as the fourth entry in the ϵ^{pred} column.

The $1/N$ dependence. The coefficient R_{13} together with ϵ_3 leads to predict the emittance of case (a). This case is for a chip model with 50 K stages and has a comparable phase, i.e., 0.16 rad. Based on the $1/N$ behavior of Eq. (56), the predicted emittance growth for case (a) should be roughly $1/50$ times of $\epsilon_3 \sim 100\epsilon_0$, i.e., $\Delta\epsilon_1 \sim 2\epsilon_0$. In turn, the estimated final emittance for case (a) is $\epsilon_1^{\text{est}} = \Delta\epsilon_1 + \epsilon_0 \sim 3\epsilon_0$. A more careful study gives the predicted value $\epsilon_1^{\text{pred}} \sim 3.2\epsilon_0$. This is the second entry under the ϵ^{pred} column. This predicted value is to be compared to $\epsilon_1 = 3.3\epsilon_0$, which is adjacent to it under the

ϵ column. The latter is obtained through direct model calculation. The approximate agreement in this comparison demonstrates that the $1/N$ factor is operative here.

The $(\sin\psi)$ law. Following the same approach, the quantities ϵ_3 and R_{43} lead to the predicted value $\epsilon_4^{\text{pred}} \sim 16.0\epsilon_0$. This is compatible to the entry $\epsilon_4 = 14.5\epsilon_0$, which is adjacent to it under the ϵ column. The approximate agreement is expected since the validity of $(\sin\psi)^{3/2}$ law for the horn model has already been established in Fig. 11. We recall that the same demonstration for the chip model has been given in Fig. 4. In other words, we also expect for case (b) $\epsilon_2^{\text{pred}} \sim \epsilon_2$. From Table II, one sees that this is indeed the case.

From horn back to CTHY. The use of ϵ_3 and the coefficient R_{03} leads to the prediction $\epsilon_{\text{CTHY}}^{\text{pred}} \sim 231\epsilon_0$. This is to be compared with the corresponding value of CTHY model, $\epsilon_{\text{CTHY}} \sim 140\epsilon_0$. So the agreement is within a factor of 2. Notice that here the predicted value based on Eq. (57) is higher than the corresponding CTHY value. The same trend is also seen Fig. 11. Notice that at the abscissa coordinate of the CTHY case, the line which is based on the $\sin\psi^{3/2}$ law is higher than the point computed by the horn model. These examples demonstrate a general overall consistency in the numerical analysis among the chip model, the horn model, and the CTHY model.

As mentioned earlier, for the chip model, its resilience against jitters is at the expense of introducing more lasers. Still, it is worthwhile to point out that the spatial interval of one acceleration stage of the chip model considered is on the order of 1 cm. This space can be further reduced either with a higher field gradient or with the increase of the number of chips.

Based on Katsouleas's matching condition, we have presented the analytic results of the horn model with synchronous acceleration. Also, the conservation of energy and the adiabatic invariance constraints have been included in the model. Here the number of laser pulses involved is much less than the chip model, and it is comparable to that of the CTHY model. Thus the horn model is more promising for experimental implementation.

Assmann and Yokoya [7] have given a qualitative estimate on the emittance degradation per acceleration stage in the case where there is a full filamentation in the transverse phase space, which is given by

$$\frac{\Delta\epsilon_{\text{unit}}}{\epsilon_0} \sim \left(\frac{\sigma_D}{x_0}\right)^2, \quad (58)$$

where ϵ_0 is the initial emittance, σ_D is the jitter parameter, or the offset parameter, and x_0 is the initial transverse radius of the beam which is determined based on the initial emittance and the betatron frequency of the system; see Eq. (19). For several cases of the horn model presented, $\sigma_D = 0.1$ μm and x_0 ranges from 0.05 to 0.08 μm. So the maximum percentage degradation per stage is at least several times greater than unity. On the other hand, for all cases considered in the present work including the CTHY model, this ratio is small compared to unity. This implies that at least there is a significant portion of the system where the transverse phase space is not in the full filamentation region. So the behavior of the emittance of the system is more complex. This justifies, *a posteriori*, why it is necessary to carry out the numerical simulation work.

In this work for the longitudinal phase spread we have used the CTHY value, i.e., $\sigma_\psi = 0.01$ rad. This gives a narrow longitudinal beam width, i.e., $\sigma_z = k_p \sigma_\psi \approx 0.2$ μm, where $\lambda_p = 100$ μm was used. There are pros and cons for this choice. On the one hand, the smallness of the bunch length helps to optimize the collider luminosity, maintain the quality of the beam profile, and keep all the beam particles within the acceleration region. On the other hand, from an experimental point of view, it is hard to prepare such a short electron bunch.[9]

We have also run a case with $\sigma_\psi = 0.02$ rad. Here, due to the additional beam spread, about 2% of the beam particles are found to be outside of the quarter-wave region. As the longitudinal beam spread is increased from 0.01 to 0.02 rad, the corresponding final emittance is found to increase from $14\epsilon_0$ to $16.8\epsilon_0$. The change is relatively small. It does not alter the main conclusion of the present paper. We will leave the investigation of using larger σ_z values and the effect of the beam loss to the future.

There is another important factor which we have not considered, i.e., the emittance growth due to multiple scattering. While the inclusion of the multiple scattering effect is outside of the scope of the present work, it is important to take it into account in a more realistic study of emittance degradation work. Based on the estimate of Montague and Schnell [22], emittance degradation due to multiple scattering increases with the decrease of the acceleration phase. They found that for a TeV laser-wakefield accelerator, the multiple scattering effect is several times greater than the initial emittance of 2.2 nm used in the present work. This aspect is left to future investigation.

ACKNOWLEDGMENTS

APPENDIX: A STEADY FLOW THROUGH A NOZZLE

The following setup is discussed by Landau and Liftshitz [16]. Consider a steady isentropic (adiabatic) fluid flow from a reservoir through a nozzle, which may be defined as a tube with a variable cross section along its axis. Assume the gas flow is uniform over the transverse cross section of the tube, and the velocity is essentially parallel to the axis of the tube. For this to be the case, the tube must not be too wide and the cross sectional area A must vary fairly slowly along its length. Denote ρ and v to be, respectively, the local fluid density and the flow velocity along the nozzle and ρ_0 is the fluid density within the reservoir. It can be shown that the normalized density function along the nozzle is given by

$$x \equiv \frac{\rho}{\rho_0} = \left[1 - \frac{1}{2}(\gamma - 1) \frac{v^2}{c_0^2} \right]^{1/(\gamma-1)}, \qquad \text{(A1)}$$

where γ is the ratio of the specific heat at a constant pressure to that at a constant volume. For a monotonic gas $\gamma = 5/2$, and for a diatomic gas $\gamma = 7/2$. The velocity of sound within the reservoir is $c_0 = p_0/\rho_0$. For a steady flow, the rate of flow is constant, i.e.,

$$Q = \rho A v = x \rho_0 A v. \qquad \text{(A2)}$$

Using the relation $v = Q/(x\rho_0 A)$, one obtains

$$1 - x^{\gamma-1} = \frac{\gamma - 1}{2} \left(\frac{Q}{x\rho_0 A c_0} \right)^2. \qquad \text{(A3)}$$

This shows that, for fixed Q, between x and A there is only one independent variable. Next, evaluate the expression at $x = x_1$, where the corresponding cross section is minimum, i.e., $A = A_{\min}$. After some algebra, it leads to

$$A f(x) = A_{\min} f(x_1), \quad \text{where } f(x) = \frac{1}{x\sqrt{1 - x^{\gamma-1}}}. \qquad \text{(A4)}$$

The plot of A versus x is given in Fig. 8 (flow) for both the monoatomic and diatomic cases. Here the extreme occurs where the local velocity equals the velocity of sound. Euler's equation implies

$$\frac{d\rho}{dv} = -\frac{\rho v}{c^2}. \qquad \text{(A5)}$$

Thus, the negative sign implies that to the left of the extremum as ρ decreases, v increases; i.e., it is in the supersonic region. On the other hand, to the right of

[9]Recent theoretical results presented by Max Zolotorev at AAC 2000, Santa Fe, indicates the possibility of obtaining electron bunch length in the submicron range.

the extremum, as ρ increases, v decreases. This region corresponds to the subsonic region. In this latter region, as the cross section A increases, x (i.e., the density) increases. Thus, one way to achieve a gradual increase of the density within a tube along the beam direction is to set up a steady flow of the fluid in the opposite direction. The downstream side of the tube is connected to a reservoir which is at the density ρ_0. Here there is a monotonic relationship; i.e., as $A/A_{\min}$ increases $x = \rho/\rho_0$ increases also. Using the $f(x)$ function, the desired density profile along the beam may be achieved through variation of the corresponding cross section value.

---

[1] T. Tajima and J. M. Dawson, Phys. Rev. Lett. **43**, 267 (1979).

[2] E. Esarey, P. Sprangle, J. Krall, and A. Ting, IEEE Trans. Plasma Sci. **24**, 252 (1996).

[3] T. Tajima, S. Cheshkov, W. Horton, and K. Yokoya, in *Advanced Accelerator Concepts: Eighth Workshop,* edited by Wes Lawson, AIP Conf. Proc. No. 472 (AIP, New York, 1999), p. 153.

[4] S. Cheshkov, T. Tajima, W. Horton, and K. Yokoya, in *Advanced Accelerator Concepts: Eighth Workshop* (Ref. [3]), p. 343.

[5] S. Cheshkov, T. Tajima, W. Horton, and K. Yokoya, Phys. Rev. ST Accel. Beams **3**, 071301 (2000).

[6] M. Xie, T. Tajima, K. Yokoya, and S. Chattopadhyay, in *Advanced Accelerator Concepts: Seventh Workshop,* edited by S. Chattopadhyay, J. McCullough, and P. Dahl, AIP Conf. Proc. No. 398 (AIP, New York, 1997), p. 233.

[7] R. Assmann and K. Yokoya, Nucl. Instrum. Methods Phys. Res., Sect. A **410**, 544 (1998).

[8] T. Chiou, T. Katsouleas, C. Decker, W. Mori, J. Wurtele, G. Shvets, and J. Su, Phys. Plasmas **2**, 310 (1995).

[9] G. Shvets, J. Wurtele, T. Chiou, and T. Katsouleas, IEEE Trans. Phys. Plasma Sci. **24**, 351 (1996).

[10] C. Chiu, S. Cheshkov, and T. Tajima, Beam Dynamics Newsletter **21**, 110 (2000). (Correction: The collider energy in this work should be at 6 TeV).

[11] D. L. Fisher and T. Tajima, Phys. Rev. Lett. **71**, 4338 (1993).

[12] Levi Shachter, Phys. Rev. E **53**, 6427 (1996).

[13] E. Yablonovitch and T. J. Gmitter, Phys. Rev. Lett. **63**, 1950 (1989).

[14] S. Kawakami, T. Kawashima, and T. Sato, Appl. Phys. Lett. **74**, 463 (1999).

[15] T. Katsouleas, Phys. Rev. A **33**, 2056 (1986).

[16] L. D. Landau and E. M. Lifshitz, *Fluid Mechanics* (Pergamon Press, New York, 1987), 2nd ed., Secs. 83 and 97.

[17] W. Horton and T. Tajima, Phys. Rev. A **34**, 4110 (1986).

[18] H. H. Kuehl, C. Y. Zhang, and T. Katsouleas, Phys. Rev. E **47**, 1249 (1993).

[19] E. Esarey, A. Ting, P. Sprangle, and G. Joyce, Comments Plasma Phys. Control. Fusion **12**, 191 (1989).

[20] M. C. Wang and G. E. Uhlenbeck, Rev. Mod. Phys. **17**, 323 (1945).

[21] G. Shvets, N. J. Fisch, A. Pukhov, and J. Meyer-ter-Vehn, Phys. Rev. E **60**, 2218 (1999).

[22] B. W. Montague and W. Schnell, in *Laser Acceleration of Particles*, edited by Chan Joshi and Thomas C. Katsouleas, AIP Conf. Proc. No. 130 (AIP, New York, 1985), p. 146.